Journal of Solid State Chemistry 184 (2011) 2941–2947

Contents lists available at SciVerse ScienceDirect

Journal of Solid State Chemistry

journal homepage: www.elsevier.com/locate/jssc

Synthesis, structural characterization and magnetic properties of RE_2MgGe_2 (RE=rare-earth metal)

Nian-Tzu Suen, Paul H. Tobash, Svilen Bobev*

Department of Chemistry and Biochemistry, University of Delaware, Newark, DE 19716, USA

ARTICLE INFO

Article history:
Received 19 August 2011
Received in revised form
31 August 2011
Accepted 4 September 2011
Available online 10 September 2011

Keywords:
Polar intermetallics
Crystal structure
Single-crystal X-ray diffraction
Electronic structure calculations

ABSTRACT

A series of rare-earth metal–magnesium–germanides RE_2MgGe_2 (RE=Y, Nd, Sm, Gd–Tm, Lu) has been synthesized by reactions of the corresponding elements at high temperature. Their structures have been established by single-crystal and powder X-ray diffraction and belong to the Mo_2FeB_2 structure type (space group *P*4/*mbm* (No. 127), Z=2; Pearson symbol *tP*10). Temperature dependent DC magnetization measurements indicate Curie–Weiss paramagnetism in the high-temperature regime for all members of the family, excluding Y_2MgGe_2, Sm_2MgGe_2, and Lu_2MgGe_2. At cryogenic temperatures (ca. 60 K and below), most RE_2MgGe_2 phases enter into an antiferromagnetic ground-state, except for Er_2MgGe_2 and Tm_2MgGe_2, which do not undergo magnetic ordering down to 5 K. The structural variations as a function of the decreasing size of the rare-earth metals, following the lanthanide contraction, and the changes in the magnetic properties across the series are discussed as well.

1. Introduction

The research of rare-earth metal silicides and germanides has drawn considerable attention in recent years [1–5]. This is due to the myriad of interesting physical properties exhibited by many such compounds, which are intricately related to their structure [2]. Motivated by the prospects for advanced technological applications and driven by the scientific curiosity to understand the relationship between structure and properties, we began exploring the ternary *RE*–Mg–Ge systems. Our initial interest into these phase diagrams was first brought about when the $Yb_{5-x}Mg_xGe_4$ compound ($x \approx 1.0$) with mixed-valent Yb^{2+}/Yb^{3+} was serendipitously discovered several years ago [3]. With the identification of Yb_4MgGe_4 (Gd_5Si_4 type, space group *Pnma*, Pearson symbol *oP*36), as part of our ongoing efforts within this research theme, we logically set out to investigate the crystal chemistry of the other rare-earth metal congeners. Through these attempts we came across the extended series with a general formula $RE_{5-x}Mg_xGe_4$ ($1 \leq x \leq 2.3$; RE=Gd–Lu, Y) [4]. Although all $RE_{5-x}Mg_xGe_4$ phases are formally solid-solutions, their structures were shown by us experimentally [4], and by others computationally [5], to exhibit preferred replacement of the rare-earth metal for Mg on one of the three available crystallographic positions. Such substitutions bring down the overall valence electron count, and cause subtle changes to the Ge–Ge and metal–metal bonding. While trying to establish the limits of the homogeneity ranges in these phases, another series of ternary compounds was recognized, namely RE_2MgGe_2 (RE=Y, Nd, Sm, Gd–Tm, Lu), crystallizing with a closely related structure (Mo_2FeB_2 type, space group *P*4/*mbm*, Pearson symbol *tP*10) [6]. The syntheses, the crystal chemistry and the bulk magnetic properties of these materials are the subject of the paper.

2. Experimental

2.1. Synthesis

All starting materials for the preparation of RE_2MgGe_2 (RE=Y, Nd, Sm, Gd–Tm, Lu) were purchased from common chemical vendors, and stored and handled inside an argon-filled glove box to prevent unwanted deterioration from moisture and oxygen. Rare-earth metals (ingots, 99.9 wt% from Ames Laboratory or Alfa-Aesar), Ge (powder, 99.999 wt% from Acros), and Mg (turnings, 99.8 wt% from Alfa) were used as received. Reactions were carried out by loading stoichiometric amounts of the respective elements inside Nb containers, sealed at both ends with an arc-welder. Subsequently, the Nb containers were enclosed in evacuated (*ca.* 10^{-5} Torr) fused silica jackets by flame sealing. The synthesis followed the standard solid-state route through crystallization from a melt, although the process was somewhat complicated due to the very high melting points of some of the rare-earth metals (greater than 1500 °C) and the relatively low boiling point of Mg (1090 °C) [7]—this greatly increased the difficulty of obtaining pure

* Corresponding author. Fax: +302 831 6335.
E-mail address: bobev@udel.edu (S. Bobev).

0022-4596/$ - see front matter © 2011 Elsevier Inc. All rights reserved.
doi:10.1016/j.jssc.2011.09.003

compounds. After many trials, the best synthetic procedure was established to be: (1) heating to 1100 °C at a rate of 200 °C/h; (2) homogenization at 1100 °C for 20 h; followed by (3) cooling to room temperature at a rate of 50 °C/h. This method afforded phase-pure polycrystalline material for RE_2MgGe_2 (RE=Y, Nd, Sm, Gd–Tm, Lu). The same synthetic route, however, was found unsuitable for synthesizing RE_2MgGe_2 compounds of the early rare-earth metals La, Ce, and Pr. They are known from previous studies [8], which have shown that induction melting yields better results than convection heating. The nominally divalent Eu and Yb do not appear to form compounds with this structure under the investigated conditions.

Attempts to grow crystals for resistivity measurements via flux reactions were unsuccessful. Several fluxes were tried – Mg, Pb, and Mg/Pb mixture – and the products were simple RE-Mg and RE-Pb binaries [6].

2.2. X-ray crystallography

X-ray powder diffraction patterns were collected at room temperature on a Rigaku MiniFlex powder diffractometer using Cu $K\alpha$ radiation (wavelength 1.54056 Å). Typical data collection included $\theta-\theta$ scans with step size 0.05° and 10 s/step counting time. Data analysis was done using the JADE 6.5 software package. The powder patterns for the products of reactions with RE=Y, Nd, Sm, Gd–Tm, Lu (following the optimized procedure above) showed single-phase RE_2MgGe_2 materials, while all syntheses aimed at the RE_2MgGe_2 (RE=La–Pr) phases resulted in complex mixtures of phases, which include the new compounds $RE_4Mg_5Ge_6$ (RE=La–Pr) [9] and $REGe_{2-x}$ [6]. The observed peak-positions and the peaks' relative intensities matched well with those calculated from the single-crystal work. For the samples used in the magnetization measurements, the purity of the material was ensured by qualitative peak-profile fits of the powder patterns. A representative powder pattern showing the calculated and the observed intensities is provided as supporting information.

According to powder patterns collected for specimens kept under inert atmosphere and to those collected after 6 months exposure to air, the title compounds are air-stable over this period of time.

Crystals of the title compounds were selected under an optical microscope, cut to desired dimensions, and mounted on glass fibers with Paratone-N oil. Full spheres of reciprocal data were collected on a Bruker SMART CCD-based diffractometer (monochromatized Mo $K\alpha$ radiation, λ=0.71073 Å). Preliminary rotation images were acquired to access the crystal quality. Data acquisition and integration were done using the programs SMART [10] and SAINTplus [11], respectively. Semi-empirical absorption correction was fixed using SADABS [12]. The structures were refined with full-matrix least square on F^2, as implemented in SHELXTL [13]. Refined parameters included the scale factor, extinction coefficients, atomic positions with the corresponding anisotropic displacement parameters. Relevant details of the crystallographic investigations are listed in Tables 1 and 2. Final atomic coordinates, equivalent isotropic displacement parameters and selected interatomic distances are given in Tables 3 and 4. CIFs have also been deposited with Fachinformationszentrum Karlsruhe, 76344 Eggenstein–Leopoldshafen, Germany, (fax: (49) 7247–808-666; e-mail: crysdata@fiz.karlsruhe.de) with depository numbers: CSD-423449 for Nd_2MgGe_2, CSD-423451 for Sm_2MgGe_2, CSD-423450 for Tb_2MgGe_2, CSD-423452 for Dy_2MgGe_2, CSD-423453 for Ho_2MgGe_2, CSD-423456 for Er_2MgGe_2, CSD-423454 for Tm_2MgGe_2, CSD-423455 for Lu_2MgGe_2, and CSD-423457 for Y_2MgGe_2.

2.3. Magnetization measurements

The DC magnetization measurements were carried out using a Quantum Design MPMS SQUID magnetometer from 5 to 300 K in a magnetic field of 500 Oe. The samples were loaded in plastic straws and secured with quartz wool in order to keep the material immobilized during the measurement. Samples from different reaction batches were measured in order to provide reproducible and reliable data. The calculated net effective magnetic moments, and the corresponding Weiss constants and Néel temperatures are summarized in Table 5.

3. Results and discussion

3.1. Structure and chemical bonding

RE_2MgGe_2 (RE=Y, Nd, Sm, Gd–Tm, Lu) crystallize in the tetragonal space group $P4/mbm$ (No. 127, Z=2). The structure is isotypic with the Mo_2FeB_2 structure [6], an ordered ternary variant of U_3Si_2, which has a Pearson symbol $tP10$ (Table 1). This structure type has been studied extensively, therefore, only a brief discussion about the structure will be given here.

This structure includes three crystallographically unique atoms in the asymmetric unit, all in special positions (Table 3).

Table 1
Selected single-crystal data collection and structure refinement parameters for RE_2MgGe_2 (RE=La, Nd, Sm, Tb, and Dy). Crystallographic data for Ce_2MgGe_2 and Pr_2MgGe_2 can be found in Ref. [8]; single-crystal structure of Gd_2MgGe_2 is reported in Ref. [19].

Empirical formula	La_2MgGe_2	Nd_2MgGe_2	Sm_2MgGe_2	Tb_2MgGe_2	Dy_2MgGe_2
Formula weight, Z=2	447.31	457.97	470.19	487.33	494.49
Crystal system			Tetragonal		
Space group			$P4/mbm$ (No. 127)		
Temperature (K)			200 K		
Unit cell dimensions (Å)	a=7.5698(14)	a=7.4124(8)	a=7.3427(9)	a=7.2494(8)	a=7.2260(3)
	c=4.4864(17)	c=4.3634(6)	c=4.3146(10)	c=4.2473(9)	c=4.2249(4)
Volume (Å^3)	257.08(12)	239.74(5)	232.62(7)	223.21(6)	220.60(2)
Density (calculated, g cm^{-3})	5.768	6.344	6.713	7.251	7.444
Absorption coefficient (cm^{-1})	277.9	336.4	375.9	445.5	468.9
Data/parameters	199/12	184/12	178/12	176 /12	174/12
R[a] indices ($I>2\sigma_I$)	$R1$=0.0160	$R1$=0.0178	$R1$=0.0132	$R1$=0.0233	$R1$=0.0138
	$wR2$=0.0453	$wR2$=0.0377	$wR2$=0.0287	$wR2$=0.0452	$wR2$=0.0296
R[a] indices (all data)	$R1$=0.0175	$R1$=0.0198	$R1$=0.0134	$R1$=0.0237	$R1$=0.0147
	$wR2$=0.0467	$wR2$=0.0390	$wR2$=0.0288	$wR2$=0.0459	$wR2$=0.0298
Goodness-of-fit on F^2	0.975	1.023	1.232	1.136	1.122
Largest diff. peak/hole (e$^-$ Å^{-3})	1.338/−0.588	1.077/−1.310	1.437/−0.568	1.376/−1.254	0.926/−0.872

[a] $R1=\sum\|F_o|-|F_c\|/\sum|F_o|$; $wR2=[\sum[w(F_o^2-F_c^2)^2]/\sum[w(F_o^2)^2]]^{1/2}$, where $w=1/[\sigma^2F_o^2+(A\cdot P)^2+B\cdot P]$, and $P=(F_o^2+2F_c^2)/3$; A and B–weight coefficients.

Table 2
Selected single-crystal data collection and structure refinement parameters for RE_2MgGe_2 (RE=Y, Ho, Er, Tm, and Lu).

Empirical formula	Y_2MgGe_2	Ho_2MgGe_2	Er_2MgGe_2	Tm_2MgGe_2	Lu_2MgGe_2
Formula weight, Z=2	347.31	499.35	504.01	507.35	519.43
Crystal system			Tetragonal		
Space group			*P4/mbm* (No. 127)		
Temperature (K)			200 K		
Unit cell dimensions (Å)	a=7.2344(7)	a=7.1929(8)	a=7.1628(16)	a=7.1468(18)	a=7.1036(19)
	c=4.2322(9)	c=4.2049(9)	c=4.1861(19)	c=4.168(2)	c=4.145(2)
Volume (Å^3)	221.50(6)	217.55(6)	214.77(12)	212.86(13)	209.17(13)
Density (calculated, g cm^{-3})	5.207	7.623	7.794	7.916	8.248
Absorption coefficient (cm^{-1})	393.00	495.7	524.5	551.8	609.3
Data / parameters	176/12	183/12	174/12	168/12	165/12
R[a] indices ($I > 2\sigma_I$)	$R1$=0.0209	$R1$=0.0194	$R1$=0.0178	$R1$=0.0158	$R1$=0.0130
	$wR2$=0.0359	$wR2$=0.0372	$wR2$=0.0453	$wR2$=0.0346	$wR2$=0.0287
R[a] indices (all data)	$R1$=0.0268	$R1$=0.0213	$R1$=0.0178	$R1$=0.0175	$R1$=0.0135
	$wR2$=0.0377	$wR2$=0.0377	$wR2$=0.0453	$wR2$=0.035	$wR2$=0.0290
Goodness-of-fit on F^2	1.067	1.114	1.107	1.129	1.065
Largest diff. peak/hole (e$^-$ Å^{-3})	0.844/−1.072	1.058/−1.470	1.172/−1.347	1.209/−0.973	1.379/−1.637

[a] $R1=\sum\|F_o|-|F_c\|/\sum|F_o|$; $wR2=[\sum[w(F_o^2-F_c^2)^2]/\sum[w(F_o^2)^2]]^{1/2}$, where $w=1/[\sigma^2F_o^2+(A\cdot P)^2+B\cdot P]$, and $P=(F_o^2+2F_c^2)/3$; A and B–weight coefficients.

Table 3
Selected atomic coordinates and equivalent isotropic displacement parameters (U_{eq}^a) from single-crystal structure refinements for RE_2MgGe_2.

Atom	*Wyckoff* site	x	y	z	U_{eq}
Y_2MgGe_2					
Y	4*h*	0.1775(1)	x+1/2	1/2	0.006(1)
Ge	4*g*	0.3768(1)	x+1/2	0	0.006(1)
Mg	2*a*	0	0	0	0.008(1)
La_2MgGe_2					
La	4*h*	0.1787(1)	x+1/2	1/2	0.007(1)
Ge	4*g*	0.3824(1)	x+1/2	0	0.007(1)
Mg	2*a*	0	0	0	0.010(1)
Nd_2MgGe_2					
Nd	4*h*	0.1781(1)	x+1/2	1/2	0.005(1)
Ge	4*g*	0.3791(1)	x+1/2	0	0.005(1)
Mg	2*a*	0	0	0	0.010(1)
Sm_2MgGe_2					
Sm	4*h*	0.1779(1)	x+1/2	1/2	0.006(1)
Ge	4*g*	0.3789(1)	x+1/2	0	0.006(1)
Mg	2*a*	0	0	0	0.010(1)
Tb_2MgGe_2					
Tb	4*h*	0.1775(1)	x+1/2	1/2	0.006(1)
Ge	4*g*	0.3770(1)	x+1/2	0	0.005(1)
Mg	2*a*	0	0	0	0.007(1)
Dy_2MgGe_2					
Dy	4*h*	0.1772(1)	x+1/2	1/2	0.006(1)
Ge	4*g*	0.3769(1)	x+1/2	0	0.006(1)
Mg	2*a*	0	0	0	0.008(1)
Ho_2MgGe_2					
Ho	4*h*	0.1771(1)	x+1/2	1/2	0.007(1)
Ge	4*g*	0.3764(1)	x+1/2	0	0.006(1)
Mg	2*a*	0	0	0	0.009(1)
Er_2MgGe_2					
Er	4*h*	0.1770(1)	x+1/2	1/2	0.007(1)
Ge	4*g*	0.3761(1)	x+1/2	0	0.006(1)
Mg	2*a*	0	0	0	0.010(1)
Tm_2MgGe_2					
Tm	4*h*	0.1770(1)	x+1/2	1/2	0.007(1)
Ge	4*g*	0.3795(1)	x+1/2	0	0.006(1)
Mg	2*a*	0	0	0	0.008(1)
Lu_2MgGe_2					
Lu	4*h*	0.1768(1)	x+1/2	1/2	0.007(1)
Ge	4*g*	0.3753(1)	x+1/2	0	0.007(1)
Mg	2*a*	0	0	0	0.009(1)

The atomic arrangement can be best viewed as 2-dimensional slabs of Mg and Ge atoms (anionic sub-structure), and layers of rare-earth metal atoms (cationic sub-structure) between them (Fig. 1). Within this description, one should consider the Ge–Ge dumbbells (formally Ge_2^{6-}), interconnected with square-planar Mg atom as forming flat [$MgGe_2$] layers (z=0), stacked along the c-axis with the layers at z=1/2, made of rare-earth metal cations (formally RE^{3+}). From a different point of view, the structure can be recognized as an array of face-shared trigonal prisms of rare-earth metal atoms, centered by Ge atoms, alternating with cubes of rare-earth metal atoms, centered by Mg atoms. This arrangement can be considered as a 1:1 intergrowth of CsCl- and AlB_2-like slabs with compositions REMg and REGe$_2$, respectively (Fig. 2), as discussed in an earlier publication [14].

At the outset of this discussion, we note that there are nearly 300 compounds adopting the Mo_2FeB_2 structure type, most of them involving transition metals [6,15]. There are a small number of ternary rare-earth metal silicides and germanides RE_2XTt_2 (X=*s*- or *p*-block element; Tt=Si or Ge), such as RE_2MgSi_2 [16], RE_2AlSi_2 [17], and RE_2InGe_2 [18]. The early-to-mid members of the RE_2MgGe_2 family (RE=La–Tb) have been studied, however the crystallographic work of Kraft and Pöttgen [8] only covers La_2MgGe_2, Ce_2MgGe_2, and Pr_2MgGe_2. Single-crystal structure refinements, magnetic susceptibility data, and electronic structure calculations have been reported for Gd_2MgGe_2 by Choe et al. [19]. Aside from the afore-mentioned theoretical work by Choe et al. [19], two other groups have done density functional theory (DFT) electronic structure calculations on the closely related germanides La_2InGe_2 and Ce_2InGe_2 [20]. Our account builds on this knowledge and provides structure refinements for RE_2MgGe_2 (RE=Y, Nd, Sm, Tb–Tm, Lu), as well as the magnetic susceptibilities for all synthesized materials.

The unit cell parameters decrease as follows: a=7.5698(14)–7.1036(19) Å, c=4.4864(17)–4.145(2) Å (with V=257.08(12)–209.17(13) Å^3) going from La_2MgGe_2 to Lu_2MgGe_2, and following the lanthanide contraction (Fig. 3). The cell parameters for RE_2MgGe_2 (RE=Y, Nd, Sm, and Tb) obtained by us from single-crystal X-ray crystallography are in excellent agreement with the X-ray powder diffraction data by Kraft and Pöttgen [8]. Comparison of the unit cell volumes of the RE_2MgGe_2 and RE_2InGe_2 series shows that they are very close to each other. This is somewhat unexpected since Pauling's covalent radius of In (1.421 Å) is larger than that of Mg (1.364 Å) [21]. However,

Table 4
Selected interatomic distances (Å) for RE_2MgGe_2.

Atomic pair	Distance	Atomic pair	Distance	Atomic pair	Distance
Y_2MgGe_2		La_2MgGe_2		Nd_2MgGe_2	
Y–Ge (× 2)	2.9395(8)	La–Ge (× 2)	3.1194(8)	Nd–Ge (× 2)	3.0341(6)
Y–Ge (× 4)	3.0596(6)	La–Ge (× 4)	3.2140(7)	Nd–Ge (× 4)	3.1380(5)
Y–Mg (× 4)	3.4015(4)	La–Mg (× 4)	3.5764(7)	Nd–Mg (× 4)	3.4923(3)
Y–Y	3.6321(15)	La–La	3.8310(10)	Nd–Nd	3.7333(9)
Y–Y (× 4)	3.7662(5)	La–La (× 4)	3.9378(7)	Nd–Nd (× 4)	3.8566(4)
Y–Y (× 2)	4.2322(9)	La–La (× 2)	4.4864(17)	Nd–Nd (× 2)	4.3634(6)
Ge–Ge	2.5183(17)	Ge–Ge	2.5483(14)	Ge–Ge	2.5323(16)
Ge–Mg (× 2)	2.8685(5)	Ge–Mg (× 2)	3.0237(6)	Ge–Mg (× 2)	2.9500(5)
Sm_2MgGe_2		Tb_2MgGe_2		Dy_2MgGe_2	
Sm–Ge (× 2)	2.9983(7)	Tb–Ge (× 2)	2.9493(10)	Dy–Ge (× 2)	2.9365(6)
Sm–Ge (× 4)	3.1080(5)	Tb–Ge (× 4)	3.0673(7)	Dy–Ge (× 4)	3.0540(4)
Sm–Mg (× 4)	3.4575(4)	Tb–Mg (× 4)	3.4105(4)	Dy–Mg (× 4)	3.3973(16)
Sm–Sm	3.6937(9)	Tb–Tb	3.6393(12)	Dy–Dy	3.6225(7)
Sm–Sm (× 4)	3.8212(5)	Tb–Tb (× 4)	3.7741(5)	Dy–Dy (× 4)	3.7629(2)
Sm–Sm (× 2)	4.3146(10)	Tb–Tb (× 2)	4.2473(9)	Dy–Dy (× 2)	4.2249(4)
Ge–Ge	2.5260(16)	Ge–Ge	2.520(3)	Ge–Ge	2.5170(16)
Ge–Mg (× 2)	2.9183(5)	Ge–Mg (× 2)	2.8753(7)	Ge–Mg (× 2)	2.8648(4)
Ho_2MgGe_2		Er_2MgGe_2		Tm_2MgGe_2	
Ho–Ge (× 2)	2.9208(9)	Er–Ge (× 2)	2.9064(10)	Tm–Ge (× 2)	2.8957(11)
Ho–Ge (× 4)	3.0408(6)	Er–Ge (× 4)	3.0285(8)	Tm–Ge (× 4)	3.0190(10)
Ho–Mg (× 4)	3.3818(4)	Er–Mg (× 4)	3.3675(8)	Tm–Mg (× 4)	3.3572(8)
Ho–Ho	3.6038(10)	Er–Er	3.5868(11)	Tm–Tm	3.5778(12)
Ho–Ho (× 4)	3.7461(4)	Er–Er (× 4)	3.7308(8)	Tm–Tm (× 4)	3.7227(9)
Ho–Ho (× 2)	4.2049(9)	Er–Er (× 2)	4.1861(19)	Tm–Tm (× 2)	4.1675(21)
Ge–Ge	2.514(2)	Ge–Ge	2.5099(18)	Ge–Ge	2.508(2)
Ge–Mg (× 2)	2.8499(6)	Ge–Mg (× 2)	2.8364(7)	Ge–Mg (× 2)	2.8293(9)
Lu_2MgGe_2					
Lu–Ge (× 2)	2.8759(10)				
Lu–Ge (× 4)	3.0035(9)				
Lu–Mg (× 4)	3.3382(9)				
Lu–Lu	3.5528(12)				
Lu–Lu (× 4)	3.7008(10)				
Lu–Lu (× 2)	4.1452(2)				
Ge–Ge	2.5057(18)				
Ge–Mg(× 2)	2.8093(8)				

Table 5
Relevant numeric parameters obtained from fitting the inverse susceptibility $\chi^{-1}(T)$ with a line[a] in the range 100–300 K.

Compounds	Magnetic ordering	$(J(J+1))^{1/2}$	μ_{eff} (μ_B)	θ_p (K)	T_N (K)
Nd_2MgGe_2	AFM	3.62	3.87	−16(1)	14(1)
Sm_2MgGe_2	AFM	0.84	0.84	−23(1)	13(1)
Gd_2MgGe_2	AFM[b]	7.94	8.00	−70(1)	32(1)
Tb_2MgGe_2	AFM	9.72	9.82	−42(1)	55(1)
Dy_2MgGe_2	AFM	10.63	10.67	−18(1)	24(1)
Ho_2MgGe_2	AFM	10.60	10.76	−11(1)	14(1)
Er_2MgGe_2	–	9.59	9.59	−6(1)	–
Tm_2MgGe_2	–	7.57	7.57	−6(1)	–

[a] The net effective moment for Sm_2MgGe_2 is derived by non-linear fit to the modified Curie–Weiss law. See text for details.

[b] The results from this study concerning Gd_2MgGe_2 are different from those reported by Choe et al. [19]. One way to explain it is that the quality of our samples is superior to those in the earlier study. This is evidenced by the absence of a kink in the $\chi(T)$ date at 150 K (which is clearly contributed from an impurity phase) and the obtained effective magnetic moments —8.0 μ_B in this work vs 8.2 μ_B in Ref. [19].

Pauling's electronegativity scale for Mg is 1.31, while for In it is 1.78 [21], which indicates that the In–Ge bonding should be more covalent in character than Mg–Ge. Therefore, it can be suggested that the differences in the In–Ge and Mg–Ge bond strengths account for the similar unit cell volumes of the RE_2InGe_2 and RE_2MgGe_2 compounds. The same phenomenology is also observed in the corresponding RE_2MNi_2 systems (M=In, Mg) [22].

We also provide single-crystal data for the already published La-analog, which is known to exist in a small homogeneity range as $La_{2+x}Mg_{1-x}Ge_2$ [23]. The purpose of this is two-fold: (i) to determine the extent of La–Mg mixing (if any) in our La_2MgGe_2 sample; and (ii) to establish a better correlation with the previously reported data, which had been done at different temperature than ours—295 vs 200 K, respectively. On this note, our single-crystal refinements do not show any disorder in the structure and the cell parameters "scale" very well with the ones previously reported for the stoichiometric La_2MgGe_2 [8]. The lack of La–Mg disorder here can be attributed to the different reaction techniques—heating in an induction furnace up to 1500 K and annealing at a lower temperature for 4 h vs our preparation, which employs radiative heating at 1373 K for 20 h.

The bond distances between Ge and Ge dumbbell pairs fall in the range from 2.5057(18) Å to 2.5483(14) Å (Table 4). These bond distances are slightly longer than those of isostructural RE_2InGe_2 (RE=Sm, Gd, Tb, Dy, Ho, Yb) (d=2.5012(2)–2.504(5) Å) [18c], but close to those of binary rare-earth metal germanides such as Sm_3Ge_5 (2.543(1) Å) [24] and the Zintl phase $EuGe_2$ (2.564(4) Å) [25]. The Ge–Ge distances monotonically decrease as the unit cell volume decreases from La_2MgGe_2 to Lu_2MgGe_2, also following the lanthanide contraction.

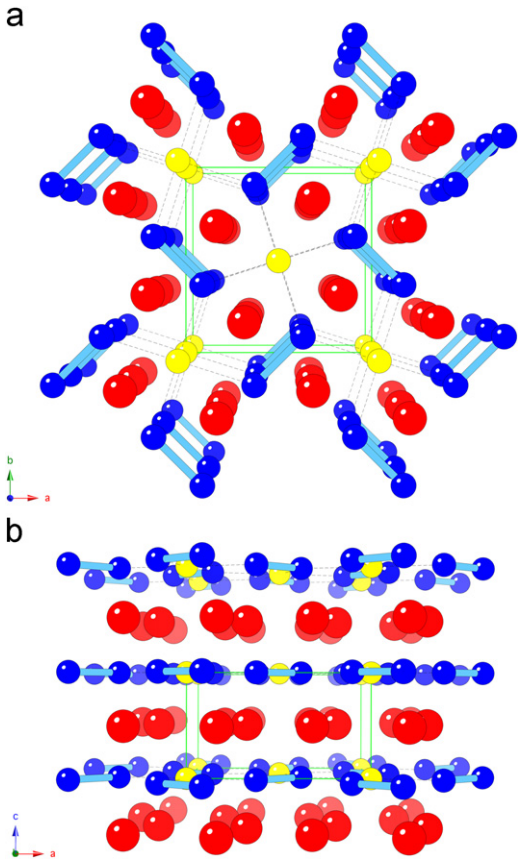

Fig. 1. Ball-and-stick representations of the primitive tetragonal structure of RE_2MgGe_2 (RE=Y, Nd, Sm, Gd–Tm, Lu) (Mo_2FeB_2 type), viewed approximately along the [001] direction (a) and approximately along the [010] direction (b). Rare-earth metal atoms are shown as red spheres, Ge atoms are represented as blue spheres, and the Mg atoms are drawn as yellow spheres. The strong covalent Ge–Ge bonds are highlighted as blue cylinders; the weaker Mg–Ge interactions are shown with dotted lines. Unit cell is outlined. (For interpretation of the references to color in this figure legend, the reader is referred to the web version of this article.)

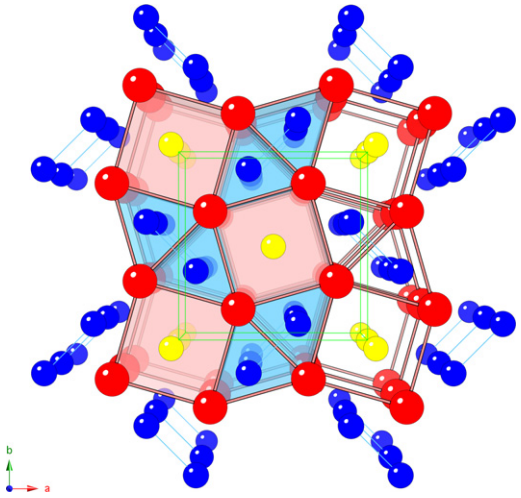

Fig. 2. Polyhedral representation of the primitive tetragonal structure of RE_2MgGe_2 (RE=Y, Nd, Sm, Gd–Tm, Lu) (Mo_2FeB_2 type), viewed approximately along the [001] direction. Rare-earth metal atoms are shown as red spheres, Ge atoms are represented as blue spheres, and the Mg atoms are drawn as yellow spheres. The trigonal prismatic REGe$_2$ fragments (AlB_2 type) and the cubic REMg fragments (CsCl type) are emphasized. For relevant interatomic distances, see Table 4. (For interpretation of the references to color in this figure legend, the reader is referred to the web version of this article.)

The Mg atoms in the structure are tightly coordinated in the *ab*-planes by four Ge atoms in a square-planar fashion (Fig. 1). The Mg–Ge contacts range from 2.8093(8) (Lu_2MgGe_2) Å to 3.0237(6) Å (La_2MgGe_2) and are substantially longer than the sum of corresponding Pauling covalent radii ($r_{Ge}+r_{Mg}$=2.608 Å) [21]. They are also longer than the Mg–Ge separation in the Zintl phase Mg_2Ge (2.76 Å) [26], which has tetrahedrally coordinated Mg. Nevertheless, according to previous electronic structure calculations by the TB-LMTO-ASA method, the Mg–Ge interactions are not weak as one could surmise and they contribute significantly to total DOS near the *Fermi* level [19].

Continuing onto the bonding and electronic structure, we discuss first the electron count following the Zintl formalism [27]. Based upon the structural information mentioned above, the Ge–Ge distances suggest this interaction to be a simple 2-center-2-electron bond. Hence, completing the valance shell of each Ge atom according to the octet rule gives the Ge_2-dimers an overall formal charge of 6−. The nature of the Mg–Ge interactions is not easily identifiable, and assigning a formal charge for Mg is not a straightforward process. One approach, as put forward by Choe et al. [19] is to rationalize the structure as $(RE^{3+})_2(Mg^{2+})(Ge_2^{6-})(2e^-)$, i.e., as a good metallic conductor with two valence electrons in the conduction band [19]. Based on work by Whangbo et al. [20], the formulation $(RE^{3+})_2(Mg^0)(Ge_2^{6-})$ can be proposed, following their arguments that the 3*s*-band of Mg is filled. Of course, this means that the family RE_2MgGe_2 (as well as RE_2InGe_2, i.e., $(RE^{3+})_2(In^0)(Ge_2^{6-})$ should be salt-like semiconductors, which disagrees with the electrical resitivity of RE_2InGe_2 (RE=Sm, Gd, Tb, Dy, Ho, Yb) [18c]. The above indicates that both ways for counting electrons are simplified approximations, which exaggerate either the ionicity or the covalency of Mg–Ge bonding.

3.2. Magnetic susceptibilities

The temperature dependent DC magnetization measurements were performed on two batch samples of RE_2MgGe_2 (RE=Y, Nd, Sm, Gd–Tm, Lu) within the range from 5 to 300 K upon both field- and zero field-cooling (applied field was 500 Oe). The data was converted to molar magnetic susceptibility ($\chi=M/H$) and are shown in Fig. 4. In the high temperature regime all samples are paramagnetic, and as expected for systems with core 4*f*-electrons, the RE_2MgGe_2 (RE=Nd, Gd–Tm) follow the Curie–Weiss law $\chi(T)= C/(T-\theta_p)$ [28], where C is Curie constant ($C=N_A\mu_{eff}^2/3k_BT$) and θ_p is the Weiss temperature. Due to the significant temperature-independent magnetism of the Sm^{3+} ion, as developed by Van Vleck [29], Sm_2MgGe_2 does not show the characteristic Curie–Weiss paramagnetic behavior. Lu_2MgGe_2 and Y_2MgGe_2 in turn both display Pauli-like temperature independent paramagnetism that can be understood as originating from the closed-shell configurations of the Lu^{3+} and Y^{3+} ions, respectively [30].

From linear fits of the inverse magnetic susceptibility vs temperature, the Curie constants for all RE_2MgGe_2 (RE=Nd, Gd–Tm) can be derived and the net effective magnetic moments (μ_{eff}) can be calculated—they are summarized in Table 5. For Sm_2MgGe_2, the significant diamagnetic core and strong Van Vleck paramagnetic contribution add a significant temperature-independent term to the susceptibility. Therefore the effective magnetic moment for the Sm^{3+} ion in this compound was calculated from a non-linear fit to the modified Curie–Weiss law, $\chi(T)=\chi_0+C/(T-\theta_p)$ [28]. The obtained values are generally in good agreement with the theoretical values for free RE^{3+} ions [28].

In the low temperature regime (ca. 60 K and below), $\chi(T)$ plots for the RE_2MgGe_2 (RE=Nd, Sm, Gd–Ho) compounds show cusp-like features, which indicate the onset of magnetic ordering and entering in antiferromagnetically (AFM) ordered states. The corresponding Néel-temperatures were determined by taking

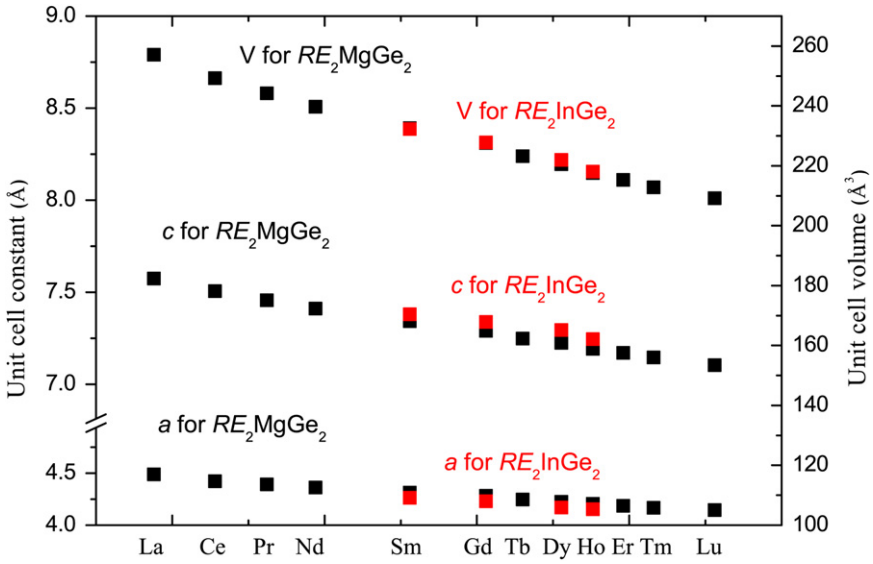

Fig. 3. Variations of the measured unit cell parameters (Å) and cell volumes (Å^3) for RE_2MgGe_2 (black) and RE_2InGe_2 (red) with the atomic size of the rare-earth metal. Cell parameters are plotted on the left *y*-axis; cell volumes are plotted on the right *y*-axis, respectively. (For interpretation of the references to color in this figure legend, the reader is referred to the web version of this article.)

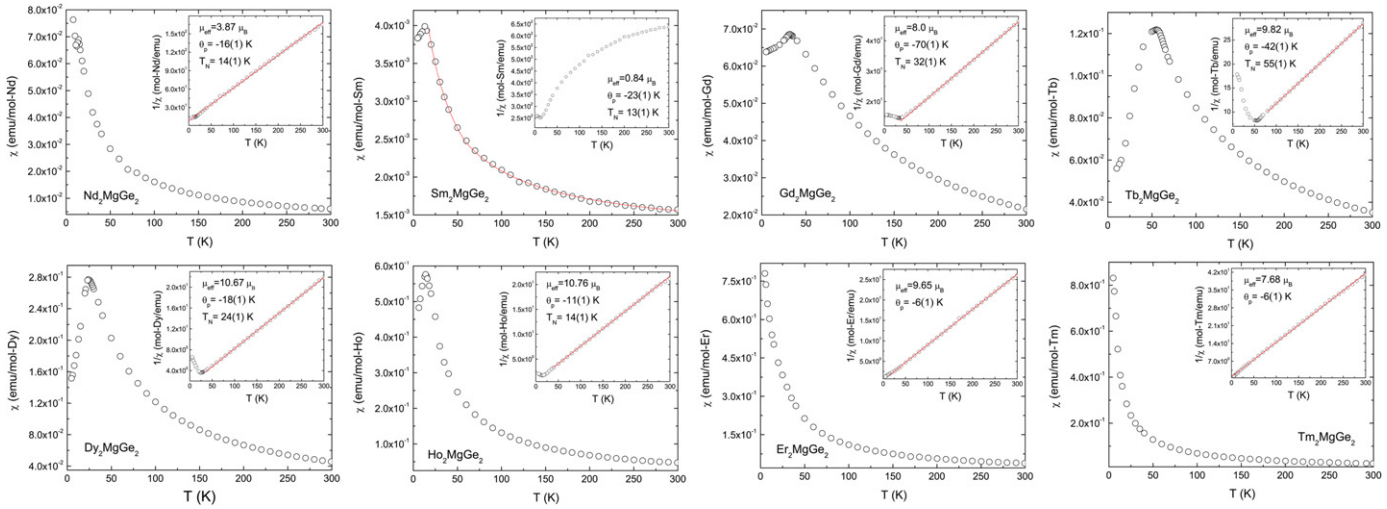

Fig. 4. Main panels: field-cooled magnetic susceptibility (χ) vs temperature of RE_2MgGe_2 (*RE*=Nd, Sm, Gd–Tm) samples. Data are gathered at 500 Oe and normalized per mol. The inset shows the temperature dependence of the inverse magnetic susceptibility. The solid line is a fit of the data to the Curie–Weiss law. Data for Y_2MgGe_2 and Lu_2MgGe_2 are not shown—χ(*T*) is temperature independent.

a derivative of dχ/dT and choosing the midpoint of the jump in dχ/d*T*. The negative Weiss constants confirm the antiferromagnetic ordering. Er_2MgGe_2 and Tm_2MgGe_2 do not appear to undergo magnetic order down to 5 K, although they may do so at lower temperature (in agreement with the DeGennes scale [31]).

The rare-earth metal atoms form planar 3^2434 nets, stacked in an eclipsed fashion. In addition, each *RE* atom is surrounded by six Ge atoms and four Mg atoms, but these polyhedra with the shape of pentagonal antiprisms are likely non-essential for the magnetic properties. As listed in Table 4, the interlayer metal–metal separation is significantly longer than the distances within the layers. Accordingly, the interactions between layers are weaker than those within the layers. Therefore, a possible magnetic structure model in low temperature is that the spins of localized 4*f*-electrons in the same layer possess the same direction (ferromagnetically coupled), while adjacent layers are antiferromagnetically coupled with each other. The mechanism for antiferromagnetic ordering in the low temperature regime is most likely due to the strong Ruderman–Kittel–Kasuya–Yodida (RKKY) interaction within the localized 4*f* electrons, mediated by the conduction electrons [28]. Choe and Miller have performed spin-polarized calculations on different magnetic structure models of Gd_2MgGe_2 and have confirmed this model to be the lowest in energy [19]. Our data agrees well with this conjecture, although to fully corroborate the proposed magnetic structure, neutron diffraction experiments are needed.

4. Conclusions

Ten ternary compounds of the form RE_2MgGe_2 (*RE*=Y, Nd, Sm, Gd–Tm, Lu) have been synthesized and structurally characterized by single-crystal X-ray and powder X-ray diffraction. Their structure has tetragonal symmetry and belongs to the ubiquitous U_3Si_2 (aka Mo_2FeB_2) structure type. The variation of unit cell constants and cell volumes across the series are in good agreement with the lanthanide contraction, as are the lengths of Ge–Ge and Mg–Ge bonds. The magnetization measurements reveal that most of the

RE_2MgGe_2 samples are Curie-like paramagnets in the high temperature range and enter antiferromagnetically ordered states at low temperature. The magnetic ordering is consistent with model spin-polarized calculations but needs to be investigated further by neutron diffraction in the future. Plans for studying the magnetic structures are under way.

Acknowledgments

Svilen Bobev acknowledges financial support from the National Science Foundation through a grant DMR-0743916 (CAREER).

Appendix A. Supplementary materials

Supplementary materials associated with this article can be found in the online version at doi:10.1016/j.jssc.2011.09.003.

References

[1] A. Szytula, J. Leciejewicz, in Handbook of Crystal Structures and Magnetic Properties of Rare Earth Intermetallics; CRC Press, Boca Raton, FL, 1994.
[2] [a] A.M. Guloy, J.D. Corbett, Inorg. Chem. 32 (1993) 3532;
[b] V.K. Pecharsky, K.A. Gschneidner Jr, Phys. Rev. Lett. 78 (1997) 4494;
[c] Y. Mozharivskyj, A.O. Pecharsky, V.K. Pecharsky, G.J. Miller, J. Am. Chem. Soc. 127 (2005) 317;
[d] A.M. Guloy, J.D. Corbett, J. Solid State Chem. 178 (2005) 1112;
[e] P.H. Tobash, G. Difiippo, S. Bobev, N. Hur, J.D. Thompson, J.L. Sarrao, Inorg. Chem. 46 (2007) 8690;
[f] P.H. Tobash, S. Bobev, J.D. Thompson, J.L. Sarrao, J. Alloys Compd. 488 (2009) 533;
[g] F. Wrubl, K.V. Shah, D.A. Joshi, P. Manfrinetti, M. Pani, C. Ritter, S.K. Dhar, J. Alloys Compd. 509 (2011) 6509.
[3] P.H. Tobash, S. Bobev, J. Am. Chem. Soc. 128 (2006) 3532.
[4] P.H. Tobash, S. Bobev, J.D. Thompson, J.L. Sarrao, Inorg. Chem. 48 (2009) 6641.
[5] S. Misra, G.J. Miller, J. Am. Chem. Soc. 130 (2008) 13900.
[6] P. Villars, L.D. Calvert (Eds.), American Society for Metals, 2nd Ed.,Materials Park, OH, USA, 1991 and the desktop edition 1997.
[7] CRCHandbook of Chemistry and Physics, 83rd ed.; CRC Press LLC: Boca Raton, FL, 2002.
[8] R. Kraft, R. Pöttgen, Monats. Chem 135 (2004) 1327.
[9] N.-T. Suen, S. Bobev, unpublished results.
[10] SMART, Bruker AXS Inc., Madison, Wisconsin, USA, 2003.
[11] SAINT, Bruker AXS Inc., Madison, Wisconsin, USA, 2003.
[12] SADABS, Bruker AXS Inc., Madison, Wisconsin, USA, 2003.
[13] SHEXLTL, Bruker AXS Inc., Madison, Wisconsin, USA, 2003.
[14] M. Lukachuk, R. Pöttgen, Z. Kristallogr. 218 (2003) 767.
[15] [a] D. Niepmann, R. Pöttgen, B. Künnen, G. Kotzyba, J. Solid State Chem. 150 (2000) 134;
[b] M. Giovannini, E. Bauer, H. Michor, G. Hilscher, A. Galatanu, A. Saccone, P. Rogl, Intermetallics 9 (2001) 481;
[c] R. Hauser, H. Michor, E. Bauer, G. Hilscher, D. Kaczorowski, Physica B 211 (1997) 230.
[16] [a] S.K. Dhar, P. Manfrinetti, A. Palenzona, J. Alloys Compd. 252 (1997) 24;
[b] R. Kraft, R. Pöttgen, Monatsh. Chem. 136 (1707 (2005);
[c] Q.-X. Xie, C. Kubata, M. Woerle, R. Nesper, Z. Anorg. Allg. Chem. 634 (2008) 2469.
[17] C. Krahnenberg, A. Mewis, Z. Anorg. Allg. Chem. 626 (2000) 1448.
[18] [a] V.I. Zaremba, A. Stepien-Damm, G.P. Nichiporuk, Yu.B. Tyvanchuk, Ya.M. Kalychak, Z. Kristallogr.—New Cryst. Struct. 212 (1997) 291;
[b] V.I. Zaremba, D. Kaczorowski, G. Nychyporuk, U.C. Rodewald, R. Pöttgen, Solid State Sci. 6 (2004) 1301;
[c] P.H. Tobash, D. Lins, S. Bobev, Chem. Mater. 17 (2005) 5567.
[19] W. Choe, G.J. Miller, E.M. Levin, J. Alloys Compd. 329 (2001) 121.
[20] [a] M.-H. Whangbo, C. Lee, J. Köhler, Angew. Chem. 45 (2006) 7465;
[b] V.I. Zaremba, D. Johrendt, U.C. Rodewald, G.P. Nychyporuk, R. Pöttgen, Solid State Sci. 7 (2005) 998.
[21] L. Pauling, The Nature of the Chemical Bond, Cornell University Press, Ithaca, NY, 1960.
[22] R.-D. Hoffmann, A. Fugmann, U.C. Rodewald, R. Pöttgen, Z. Anorg. Allg. Chem. 626 (1733 (2000).
[23] La/Mg mixed occupancy at *Wyckoff* site 2*a* has been reported only for $La_{2+x}Mg_{1-x}Ge_2$, but not for Ce_2MgGe_2 and Pr_2MgGe_2 (see Ref. [8]).
[24] P.H. Tobash, D. Lins, S. Bobev, N. Hur, J.D. Thomposon, J.L. Sarrao, Inorg. Chem. 45 (2006) 7286.
[25] S. Bobev, E.D. Bauer, J.D. Thompson, J.L. Sarrao, J. Magn. Magn. Mater. 177 (2004) 3545.
[26] V.M. Glazov, N.N. Glagoleva, Inorg. Mater. 1 (1965) 989.
[27] [a] E. Zintl, Angew. Chem 52 (1939) 1;
[b] S.M. Kauzlarich (Ed.), Chemistry, Structure and Bonding of Zintl Phase and Ions, VCH Publishers, New York, and the reference therein.
[28] J.S. Smart, Effective Field Theories of Magnetism, Saunders, Philadelphia, PA, 1966.
[29] J.H. Van Vleck, The Theory of Electric and Magnetic Susceptibilities, Oxford University Press, London, 1965.
[30] N. Spaldin, Magnetic Materials, Cambridge University Press, Cambridge, 2003.
[31] P.G. de Gennes, J. Phys. Radium 23 (1962) 510.